# Axial FLOW CHARACTERISTICS WITHIN A SCREW COMPRESSOR

D. Guerrato, J. M. Nouri, N. Stosic and C Arcoumanis
School of Engineering and Mathematical Sciences
The City University, London EC1V OHB, U.K.

**ABSRACT**

The angle-resolved mean and turbulence characteristics of the axial air flow inside a screw compressor with both male and female rotors have been measured, using a laser Doppler velocimeter (LDV) with high spatial and temporal resolution at different radial and axial locations for speeds of 800-1600 rpm, discharge pressures of 1-1.6 bar and discharge temperatures of 33-90°C. The velocity measurements were performed through a special transparent window fixed near the discharge port. The results confirmed the ability of the LDV technique to characterise the flow inside the compressor working chamber; an angular resolution of 1.5° was able to fully describe the velocity field within the machine. The flow variation between the different working chambers was established as well as the spatial variation of the axial mean velocity and turbulence velocity fluctuation within the working chamber.

The effect of discharge port opening on the axial mean and RMS velocities was found to be significant near the leading edge of the rotors causing an increase in the mean and RMS velocities of the order of $4.2V_p$ in mean (where $V_p$ is the axial pitched velocity) for male rotor and $5.4V_p$ for, female rotor and this effect is less pronounced on the flow near the root of the rotor. Moreover, to obtain a better understanding of the flow motion, a high sampling rate pressure transducer was used to provide the internal angular static pressure variation. These measurements are used to validate the in-house CFD model of the fluid flow within twin screw compressors which, in turn, allows reliable optimisation of various compressor designs.

**Keywords**: Screw Compressor, Laser Doppler Velocimetry, Cycle-resolved averaging

## INTRODUCTION

The use of screw compressors in industry is widespread since they have replaced the traditional reciprocating compressor in a large range of applications such as air compression, refrigerant compression and particularly supercharging in the automotive industry. Nowadays, due to global environmental issues, energy conservation has become a very important problem. Particularly due to the popularity of automotive engines, further reduction of exhaust emissions and improvements in fuel consumption and performance, are quite urgent requirements in every region of the world. A cost-effective solution to this problem is the addition of a power-boosting device to small engines such as a twin-screw supercharger. More generally speaking, other improvements in screw compressors are continually sought-after, in order to increase their performance, reduce their energy consumption, noise generation and manufacturing costs. A screw compressor consists of two rotors contained in a casing where their meshing lobes form a series of working chambers within which compression takes place as described in [1]. As the rotors turn, air is admitted through the space between the rotor lobes and the suction port. Further rotation of the rotor leads to cut-off of the suction port and the trapped air is pushed forward axially and circumferentially towards the discharge port by the action of the screw rotors; during this period the trapped volume in each passage is reduced and its pressure is increased. This process continues until the working volume between the rotors is exposed to the discharge port allowing gas at high pressure to flow out [1]. The performance of such compressors depends on the flow field characteristics. It is thus essential to have a good understanding of the gas flow motion in the compressor by quantifying the velocity field in the compressor elements, suction, discharge and working chambers and, especially, through the clearance gaps so as to characterise the whole sequence of processes that occur within the compressor. The total number of papers published on the flow characteristics within twin-screw compressors for superchargers is rather small in compared to

published work on other machines such as turbocharger. Moreover, the investigations of [2-3] seem to be the only reported experimental works on the flow behavior in screw compressors or screw superchargers. However, there are many experiments focusing on the performance of the compressors; for example, [1&4] describe some performance test measurements in the same compressor used for this experiment at City Compressor Centre. The material presented in this paper is part of a long-term research project attempting to measure the fluid mean velocity distribution and the corresponding turbulence fluctuations at various cross-sections of the compressor working volume within the interlobe space and at different phase angles. The aim is to reveal how major features of the fluid flow within the machine are affected by the rotor geometry and the operating conditions.

In addition to the flow measurements, other properties of the compressor such as the suction and discharge pressures and temperatures have been measured with standard laboratory-type instruments and compared with predicted values of the same properties derived from an existing CFD model [4]. This comparison has allowed validation and further development of the CFD package to a stage which renders it capable of designing future screw compressors without the need for expensive and time-consuming experiments.

As described above, the flow in screw compressors is complex, three-dimensional and strongly time-dependent similar to the in-cylinder flows in gasoline and diesel engines [5,6], centrifugal pumps [7], or in turbocharger turbines [8-10] and mixing reactors [11]. This implies that the measuring instrumentation must be robust to withstand the unsteady aerodynamic forces, have high spatial and temporal resolution and, most important, must not disturb the flow. Only point optical diagnostics like LDV can fulfill these requirements as demonstrated by previous research in similar flows. The preferred method of research is characterisation of the fluid mean velocity and turbulence fluctuations at a range of pre-selected measurement points using a dual beam Laser-Doppler Velocimeter (LDV).

The same dual beam LDV-system as that of [2,3] was used to obtain the angle-resolved axial mean and the turbulence characteristics of the flow inside the working chamber. Measurements were performed for both the male and the female rotor in the interlobe region at different radial and axial positions. That proved possible using two transparent windows made of Plexiglass (Perspex); one for the male and one for the female interlobe regions. Both were installed on the same grove close to the discharge side and were large enough to allow near backscatter light collection. The internal profile of the windows was exactly the same as that of the rotor's casing (see Figure 2(b)) in order to minimise any flow disturbance and preserve the integrity of the flow motion. The only geometric difference between the window and the casing is the roughness of the wall surface which is smoother in the case of the window. The following three sections of this paper describe the flow configuration and experimental techniques, present and discuss the results, and summarise the main findings and their implications.

## FLOW CONFIGURATION AND INSTRUMENTATION

LDV velocity measurements were obtained for a standard screw compressor. The test rig was modified to accommodate the new optical compressor, the transmitting and collecting optics and their traverses. The transparent window was machined from acrylic to the exact internal profile as the rotor casing, Figure 1(b), and is positioned at the pressure side of the compressor near the discharge port, as shown in Figure 1(a). After machining the internal and external surfaces of the window, these were fully polished to allow optical access. Angle-resolved axial velocity measurements were performed along a radial plane inside the working chambers of the male rotor near the discharge port. It is worth noting that there are five working chambers operating within a compressor rotor in a given cycle. Figure 2 shows the coordinate systems applied for each rotor where $\alpha_p$ and $R_p$ are, respectively, the angular and radial position of the control volume and $H_p$ is the distance of the control volume from the discharge port centre.

For the male rotor an angular plane of $\alpha_p=27^o$ was selected, as shown in Figure 2, and measurements were made at radial planes of $R_p$=44 to 63.2 mm and at different axial planes of $H_p$=20 to 34 mm. The corresponding measuring range of radial and axial locations for the female rotor were $R_p$=38 to 50mm, $H_p$=20 to 34mm. The direction of the measured axial velocity component is along the axes of the rotor with positive values from the suction to the discharge port.

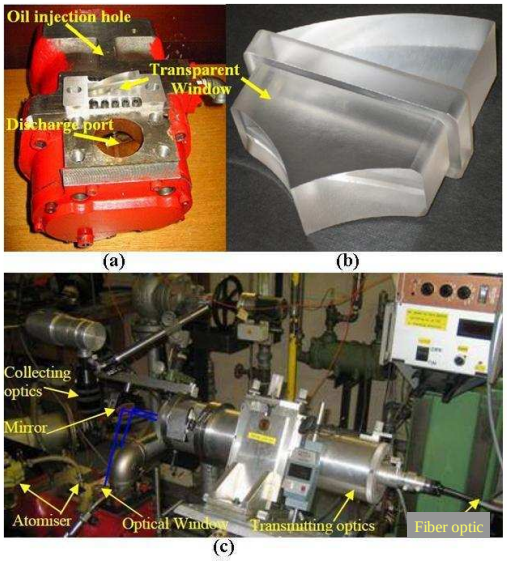


**Figure 1** Optical compressor set up: (a) modified compressor with transparent window near the discharge; (b) transparent window and its internal profile; (c) LDV optical set up of transmitting and collecting optics.

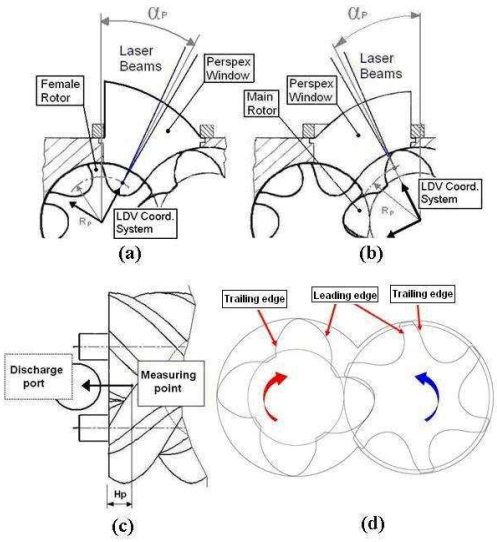


**Figure 2** Coordinate system adopted for the compressor: (a) female rotor working chamber cross-section; (c) male rotor working chamber cross-section; (c) axial plane view, (d) of male and female blades.

As explained in [2] it wasn't possible to obtain all the desired LDV measurements under oil flooded conditions. Thus, in order to be able to measure the velocity field, it was decided to run the compressor with no oil injection in the speed range of 800-1600rpm when the discharge temperature increases according to the speed and the corresponding values were: 800rpm-51±3ºC, 1000rpm-57±3ºC, 1200rpm-59±4ºC, 1400rpm-60±4ºC, 1600rpm-62±4ºC. In this way the true flow characteristics induced by the rotation of the rotors and the imposed boundary conditions, like rotors profiles and the casing, can be evaluated. Air was used as the working fluid and the flow regime was identified by the Reynolds number defined as $Re=\rho V_p D_p/\mu$ where $V_p$ is the male rotor pitch velocity (blade's velocity) calculated to be 3.152 and 6.304 m/s for rotor speeds of 800 and 1600 rpm, respectively, and $D_p$ is the male rotor pitch diameter which is 81.8 mm; for the calculation of the blade's pitched velocity the rotor's lead helix angle was 42.63 degrees. The calculated Reynolds number was found to be 14080 and 28160 for a rotor speeds of 800 and 1600 rpm, respectively, and therefore the flows under these speeds can be considered to be turbulent. The volumetric flow rates through the compressor were measured by an orifice plate installed in the exhaust pipe to be 0.880 $m^3$/min and 1.934 $m^3$/min for rotational speeds of 800 and 1600 rpm, respectively.

For the LDV application, Figure 1(c) shows the main components of the laser Doppler Velocimeter which was operating in the dual-beam near backscatter mode and comprised a 600 mW argon-Ion laser, diffraction-grating unit to divide the light beam into two and provide frequency shift, collimating and focusing lenses to form the control volume. A fiber optic was used to direct the laser beam from the laser to the transmitting optics, and a mirror was used to direct the beams from transmitting optics into the compressor through the transparent window, as shown in Figure 2 (c). The collecting optics was positioned around 25° to the full backscatter position and comprised collimating and focusing lenses, a 100 µm pin hole and a photomultiplier equipped with an amplifier. The size of the pinhole defines the effective length of the measuring volume and its diameter and fringe spacing were calculated to be 79 µm and 4.33 µm. The signal from the photomultiplier was processed by a TSI processor interfaced to a PC and led to angle-averaged values of the mean and RMS velocities. In order to synchronise the velocity measurements with respect to the location of the lobs (blades), a shaft encoder that provides one pulse per revolution and 3600 train pulses, giving an angular resolution of 0.1°, was used; it was fixed at the end of the driving shaft. Instantaneous velocity measurements were made over thousands of shaft rotations to provide sufficient number of samples; in the present study the total number of data was set differently according to the radial location of the control volume but the average sample density was 1250 data per shaft degree. Since the

TSI software is provided by 4 external channels, one of them was used to collect the pressure signal coming from the high data rate pressure transducer via an amplifier. The pressure samples were collected together with the incoming velocity and matched with the instantaneous position of the shaft.

In order to measure the flow inside the compressor, it is essential to seed the flow so that the seeding particles inside the measuring volume can scatter light from which their velocity can be obtained. The size of these particles/droplets should be small enough to ensure that all of them are following not only the mean flow but also the velocity fluctuations. For that reason, a silicone oil atomiser was used for the LDV measurements since it can produce droplet sizes in the range of 1 to 2 μm; a low viscosity silicone oil of 5 cSt was used.

A Matlab program was written in which the information of the shaft angular position from the shaft encoder was used to resolve the velocity with respect to the rotor, the so-called 'gated' measurements. This has been done by collecting the sum of all the instantaneous velocities over a given time-window (i.e. 1.5° of a revolution in this experiment) and then the ensemble mean and RMS values were calculated. This method of gated measurements proved efficient since the data was collected continuously as the rotor turned and provided ensemble averages for every 1.5° over the entire 360˚ cycle in a time interval of up to 25 minutes which, apart from a few critical points, gave the minimum amount of 600 samples per time-window corresponding to statistical uncertainties of less than 1.6% and 5.5% in the ensemble mean and RMS velocities, respectively, based on a 95% confidence level and velocity fluctuations of the order of 20% of the mean value.

## RESULTS AND DISCUSSION

The post processing technique and the choice of the most suitable resolved angle-window was already defined in [2], as well as the overlapping procedure involved in the generation of the velocity profiles. The following results show the behaviour of the axial component of velocity and the corresponding turbulence (RMS) as a function of the shaft angular position from the trailing to the leading edge of the rotor; these two edges are defined with respect to the rotation of the rotor in Figure 2(d) so that the trailing edge is placed immediately behind the moving rotor tip while the leading edge is placed in front of the blade-tip. All the presented velocity curves correspond to a particular position of the control volume in the working chamber and they have been obtained for the following parameters: Rotational speed 1000 rpm; Pressure ratio 1; Discharge temperature 55±3°C. In each figure, all the curves have been obtained at the same radial position ($R_p$) and each profile corresponds to a certain distance from the discharge port ($H_p$). All the velocity profiles in these figures present an angular shift from left (trailing edge) to right (leading edge) due the helicoidal shape of the rotors as shown in Figure 3(a).

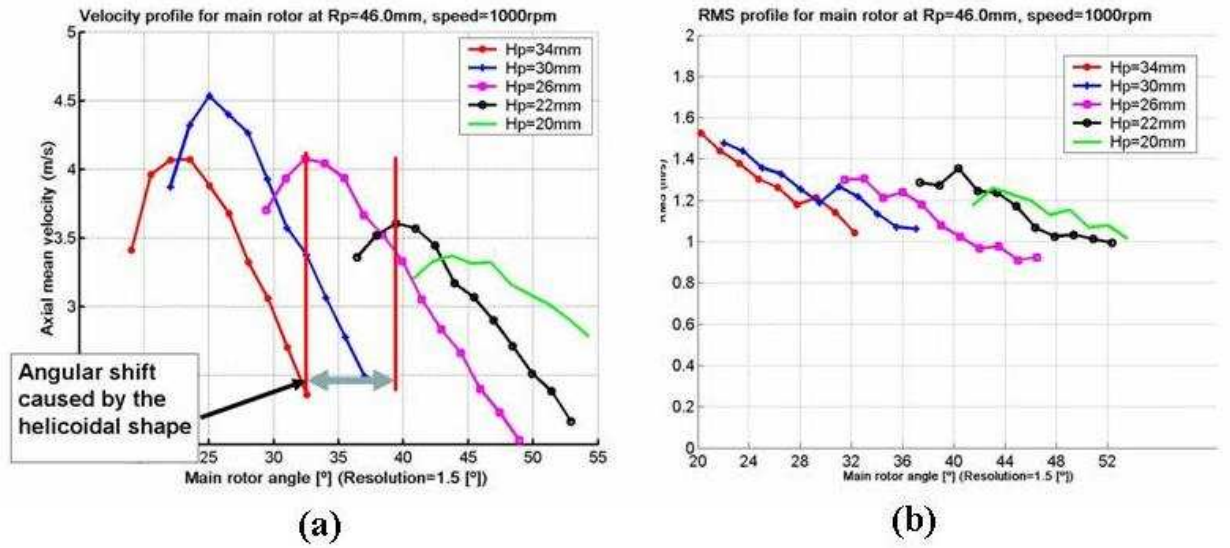


**Figure 3** Main rotor axial mean velocity diagrams at $R_p$=46.0 mm for different axial locations ($H_p$) from the discharge port: (a) mean values, (b) RMS values

The curves in Figure 3(a) also expose the mean velocity values inside the inter-lobe region of the main (male) rotor at a radial position of $R_p$=46.0 mm, i.e. near the root of the rotor. Curves have quite similar shape in all axial measurement points and show an increase in mean velocity, from the trailing edge (on the left of the graph), to a maximum and then drops towards the leading edge (on the right of the graph). It is worthy to note that in addition to the angular shift in velocity profiles, there is a decreasing offset in mean velocity magnitude as the axial measurement point moves closer to the discharge side. This can be reasonably explained taking into account the fact that the air flow motion is moving towards the upper region of the working chamber where leakages, through the rotor-case clearances, occur. Figure 3(b) shows the corresponding turbulence intensity, and in general shows a decrease in RMS values from left to right and that there is a tendency of forming peak-like profiles. Similar mean and RMS velocity profiles to those of Figure 3 are presented in Figure 4 but further away from the root of the rotor at $R_p$= 58.0 in the middle of the working chamber between the root and the tip of the main rotor region. As it can be seen from Figure 4 (a), the mean flow variation is much more complex than that shown in Figure 3(a). The results show a new aspect of flow near the leading edge that has been revealed with the latest set of experimental observations. The rapid air motion taking place immediately after the opening of the discharge port, and is mainly due to the existence of the pressure difference between the internal compression and the discharge pressure. As it is clearly evident the flow acceleration in that region is considerable and provokes an intense turbulence, looking at the Figure 4(b) an increase of up to three-fold is observed.

Since the mean flow variation in Figure 4 is large across the angular width of the working chamber from left to right then it is possible to indicate 2 different zones in which the air flow exhibits major differences:

- Zone (1) where the velocity decreases towards a defined value around the middle of the working chamber for all the curves. This common value appear for radial location of $R_p$=58.0 up to $R_p$=63.2 and it decreases with $R_p$. It should be noted that the initial stage of this zone is similar to that observed at lower radial position near the root of the rotor and displays on Figure 3.
- Zone (2) in which the velocities exhibit a sudden drop initially at angular position of 60° and then the flow is subjected to a high and consistent acceleration till it peaks and finally it decelerate.

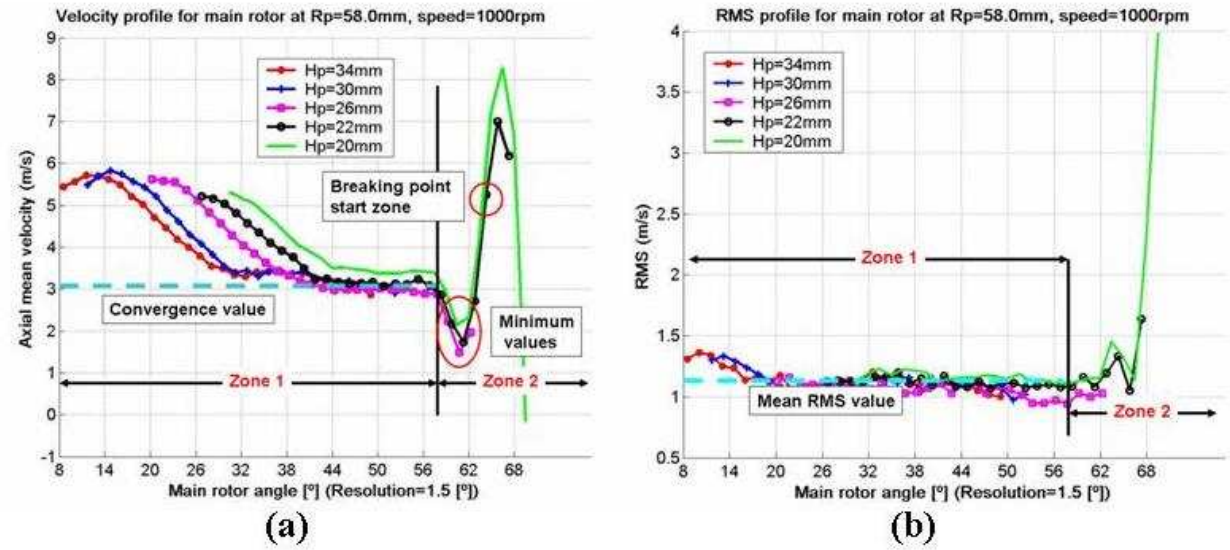


**Figure 4** Main rotor axial velocity diagrams in the middle of the interlobe region at $R_p$=58.0mm for different axial locations ($H_p$) from the discharge port: (a) mean values (b) RMS values

As mentioned before, the velocity profiles in zone 1 tends to converge on the same value and that all the curves are almost coinciding. This matching of the curves is extended to the initial part of zone 2, till the minimum value and it is also extended a bit further until a point which is identified in Figure 4(a) as the breaking point. After the breaking point the curves follow different paths which are mainly due to unsteady nature of the flow as the discharge port is opening with large pressure fluctuations, partly due to relative position of the measuring points to the discharge port, and also partly related to the LDV measurement

uncertainty limitation. With the latter point, basically when the flow from the working chamber rushes out rapidly into the discharge port, the seeding will also be dispersed rapidly along the discharge chamber. This means that only few seeding particles are available to provide data to the LDV measurements. Thus the statistical analysis is subdued to random errors. Moreover the turbulence is very high and this adds further uncertainty to the measurements.

To have a better understanding of the discharge phenomenon that was observed in Figures 4, the pressure and two velocity profiles for the cross section defined by $H_p$=20 mm are exhibited in the same plot of Figure 5. The data provide evidence of the correlation between the variation of pressure and velocity with the discharge opening.

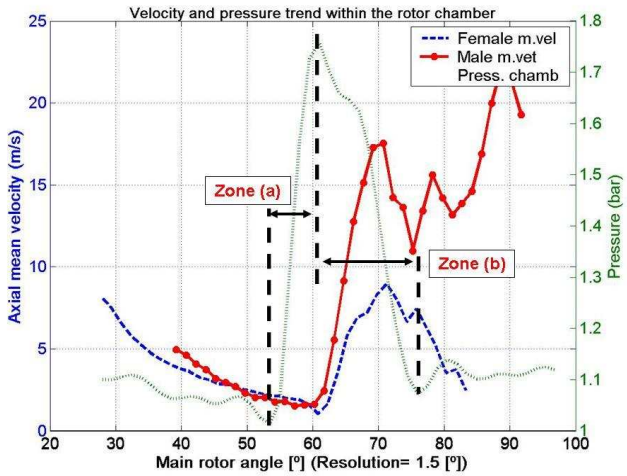


**Figure 5** Pressure and velocity distribution within the rotor chamber.

The ascending part of the pressure curve, called zone (a), displays the passage from the working chamber where discharge process is already taking place, to the next one when the process is not started yet. The descending part of the curve, named zone (b), is due to decompression of the air with opening of the discharge port. By superimposing the pressure and the velocity profiles, it has been possible to deduct that the rapid acceleration of the air flow and the quick pressure drop within the working chamber are linked together and caused by the discharge processes.

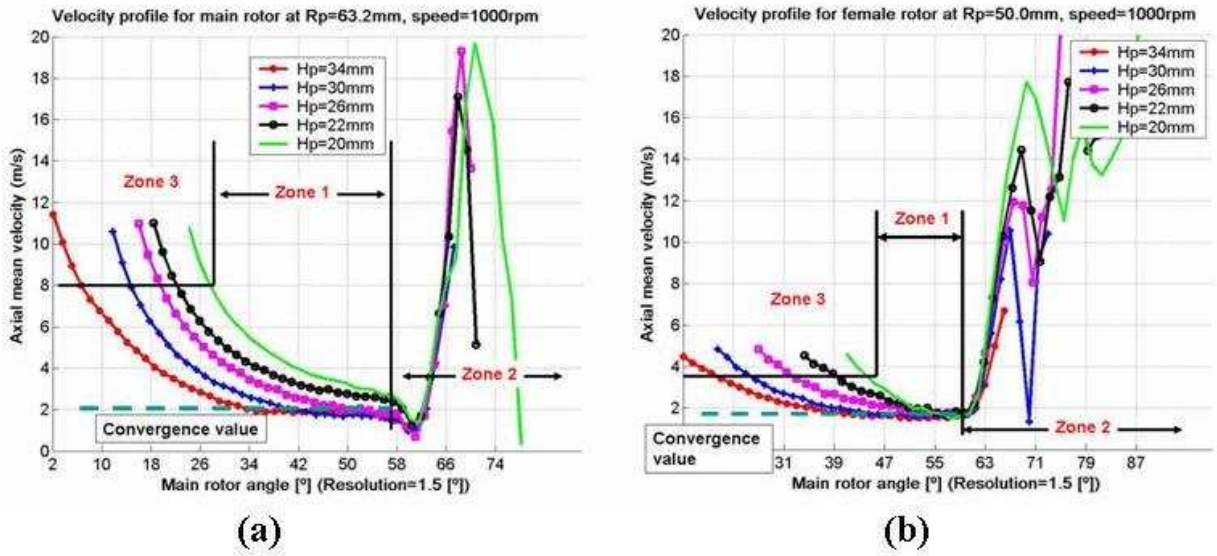


**Figure 6** Axial mean velocity profiles in the upper region of the interlobe area near the rotor tip for different axial locations ($H_p$) from the discharge port: (a) Male rotor at the radial location of $R_p$=63.2mm; (b) Female rotor at the radial location of $R_p$=50.0mm.

Another interesting feature that requires to be investigated is the flow occurring in the region close to the clearances between the rotors and the case. Figure 6(a) presents the axial mean velocity profiles near the tip of the male rotor at $R_p$=63.2mm, where the results exhibit similar mean flow variation to those observed in Figure 4(a) except on the left side of the mean flow curves near the trailing edge where a new zone can be identified. This zone is identified in Figure 6(a) and displays the velocity trends in the proximity of the trailing edge where flow losses through the gaps between working chambers take place. The velocity behaviour is the same for all the curves, so is reasonable to assume that close to the tip, the pressure difference between chambers control the flow.

In Figure 7 a representation of the axial velocity flow in the main rotor lobe is given and shows the velocity variation at three different radial positions near the root, in the middle and near the tip of the male rotor. As the control volume travels from the leading edge to the trailing edge, it is possible to track the velocity variation along some circumferential arcs. Usually, as the control volume gets close to the wall, the velocity intensity decreases, as would be expected due to no slip condition; these are the case with the velocity profiles near the root and in the middle of the rotor lobe. However, near the tip where the leakage region is, this doesn't happen and instead the velocity rises to form a jet-like profile. This is reasonably due to the flow losses through the clearance as was mentioned above and is shown in the schematic representation. That leads to a radical change not only of the value but also in the derivative of the velocity diagram close to the trailing edge.

On Figure 6(b), the experimental results inside the female rotor lobes are presented in the same manner that was shown for the male rotor. In general, the trends in mean flow are similar to those found for the male rotor on figure 6(a). The most interesting difference can be visualized close to the rotor tip on the left hand side in zone 3 where the peak velocity is lower within the female rotor and the influence of the flow rate of the air flow through the clearances is minor. This is due to the rotor profile shape, as the female rotor is characterised by a bigger tip thickness with respect to the male rotor and this reduces the flow losses from one side to another. On this region of the working chamber, turbulence on both the male and female side present the same behaviour similar to that illustrated in figure 4(b).

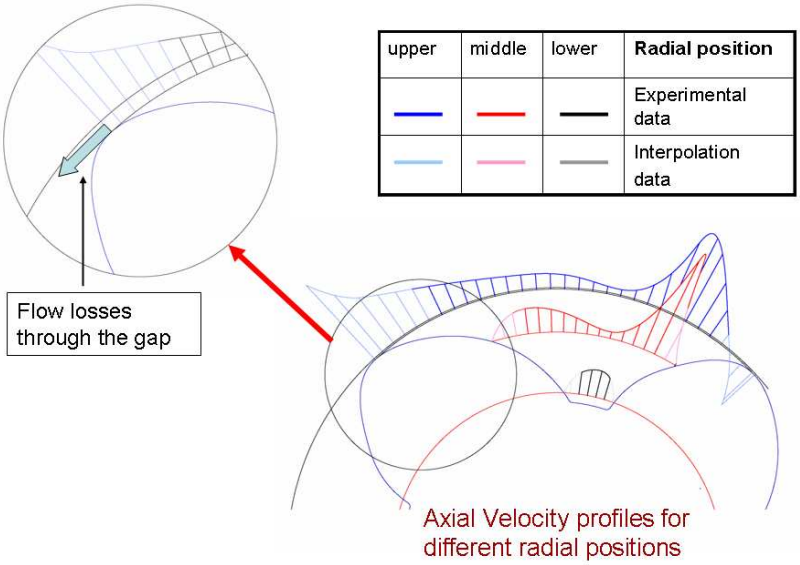


**Figure 7** Schematic representation of the angular variation of axial mean velocity profiles and flow losses with the main rotor.

It has not been possible to investigate the air flow characteristics close to the root of the rotor, because of its rounded shape. At certain angular positions, it created difficult conditions due to the mixing of the reflected light, from the base surface, with the LDV signal; this caused excessive disturbance in the signal with a very poor SNR and increased experimental error. These areas were identified, an example is shown in Figure 8, and taken into the consideration when the data were analysed. This effect was not present with the male rotor.

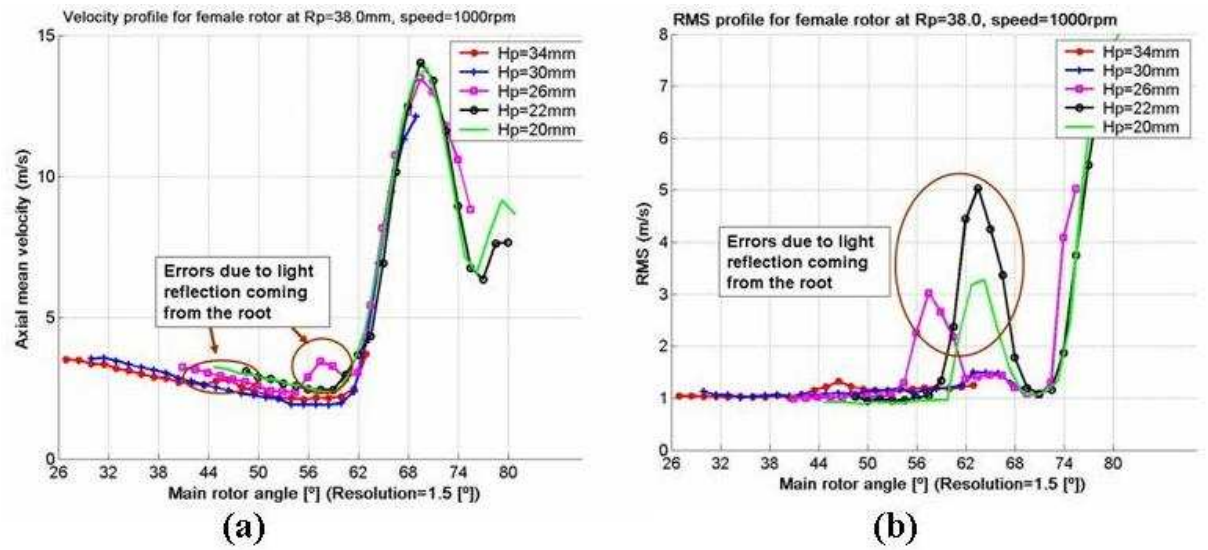


**Figure 8** Female rotor data velocity profiles near the root of the rotor at $R_p$=38.0mm for different axial locations ($H_p$) from the discharge port: (a) mean values (b) RMS values.

Figure 9 presents the effect of temperature on the mean axial velocity behaviour for a fixed location of the control volume on the male lobe part. The measuring point was chosen to be close to the internal surface of the window at $R_p$=63.2mm, $\alpha_p$=27°, $H_p$=30mm, where all the three different zones were present and the LDV signal was very good with high SNR. Looking at the picture it is possible to observe how the temperature influences the velocity profiles. In general the differences are very small particularly in zones 1 and 2, but bigger divergences can be seen in zone 3 on the left hand side. This effect is mainly due to the thermo expansion of metal and Perspex parts, causing a reduction of gap thickness. For smaller gaps between the casing and the rotor tip, the flow leakages decrease and therefore the velocity profiles close to the trailing edge are shifted down along the y-axis of the graph. In addition, is worthy to point out that for all the temperatures and far from the discharge process turbulence remains almost constant equal to 1.2 even if the air density decreases and Reynolds number raises. Moreover, comparison between values measured for both the rotors, shows similar behaviour on the axial flow.

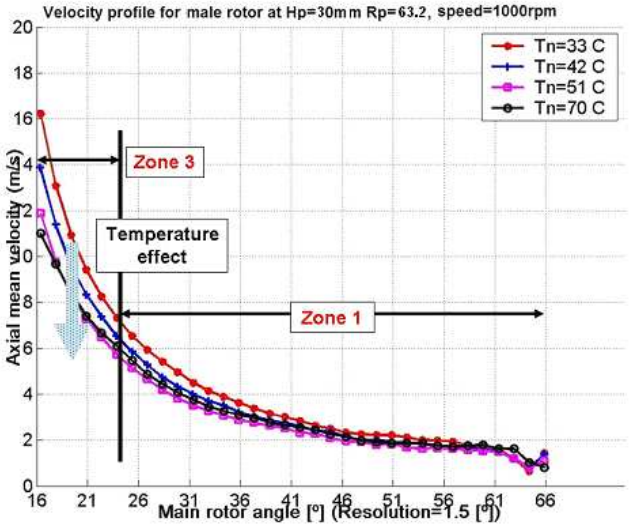


**Figure 9** Temperature influence on the axial mean velocity profiles in the male rotor: $R_p$=63.2mm and $H_p$=30mm.

Figure 10(a) and (b) show the rotor speed influence on both mean velocity and turbulence curves in the female rotor area. The control volume location is close to the rotor tip at $R_p$=50.0mm, $\alpha_p$=27° and $H_p$=30mm. A rising in speed moves the velocity curves up and it provokes a considerable increment of the turbulence inside the working chamber. Increasing of velocities and turbulences is due to the higher motion of the rotors, as well as an increment of the internal pressure which leads to stronger discharge flow from the rotors chamber. The rising of internal compression can be explained considering that for higher speed the whole compression procedure within the machine occurs in a shorter time, thus less flow escape through the gaps. Consequently, more air is confined within the same chamber volume and that provide the internal pressure increment.

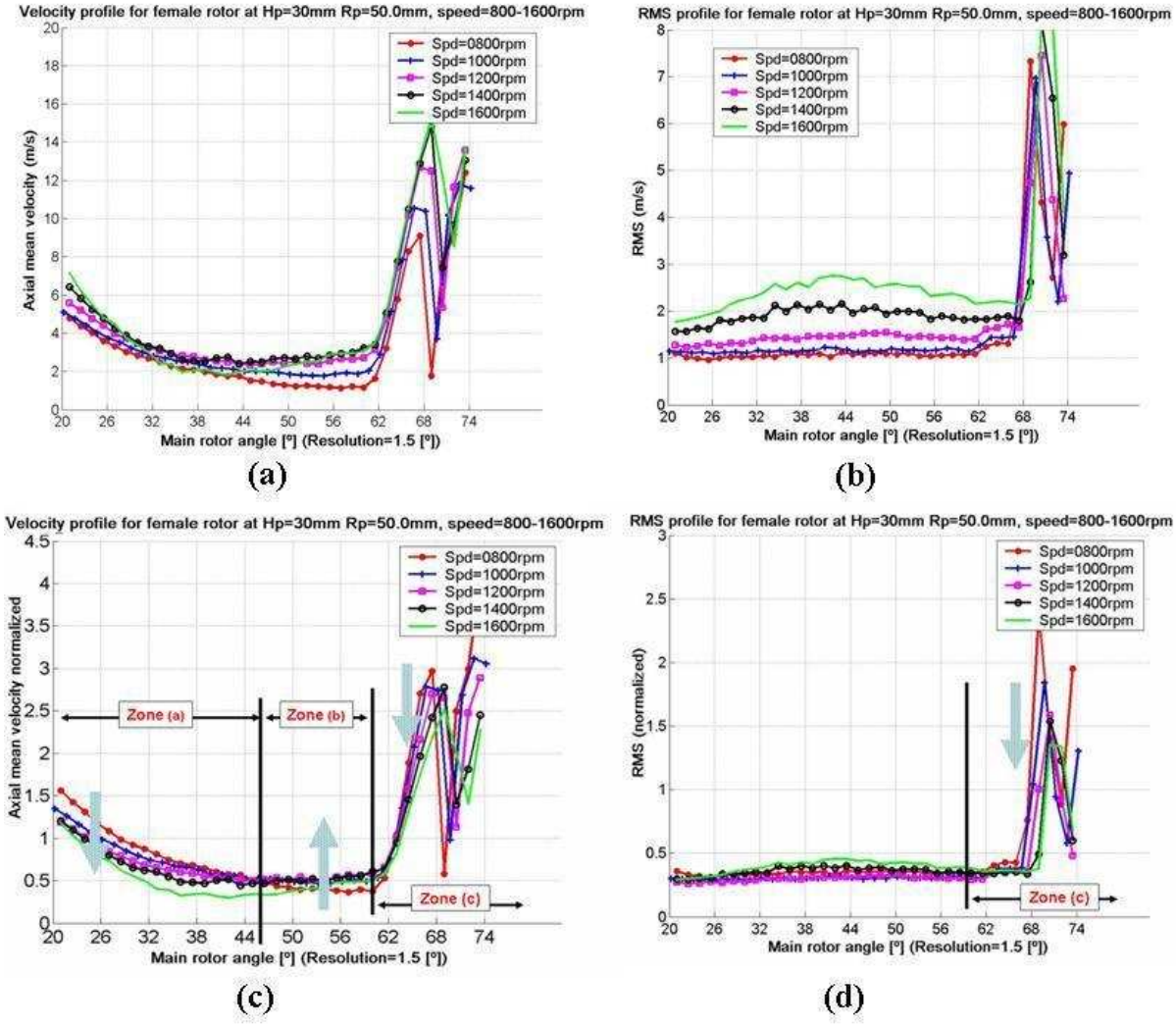


**Figure 10** Rotor speed influence in the female rotor: $R_p$=50.0mm and $H_p$=30mm: (a) axial mean velocity (b) axial RMS values (c) axial normalized mean velocity (d) axial normalized RMS values.

In order to take into account the speed effects of the compressor, in Figure 10(c) and (d) the velocity data are normalized by the main rotor speed. Normalization substantially compacts all the curves especially RMS values. However, as Figure 10(c) shows, some differences still happen before the opening of the outlet port. As it is possible to see, there are two distinct regions, zone (a) where velocity curves shifted down, especially at the rotor tip, as soon as pressure ratio goes up, and in zone (b) where an opposite trend can be seen. Zone (c) illustrates a good overlapping of the velocity profiles obtain at the discharge; here the flow motion is mainly driven by pressure difference between internal compression and outlet pressure. However, as the internal compression increases almost linearly with the compressor speed, the velocity

values also increase in a similar way. Thus, normalising the data by the compressor speed, all the curves have a tendency to follow the same trend.

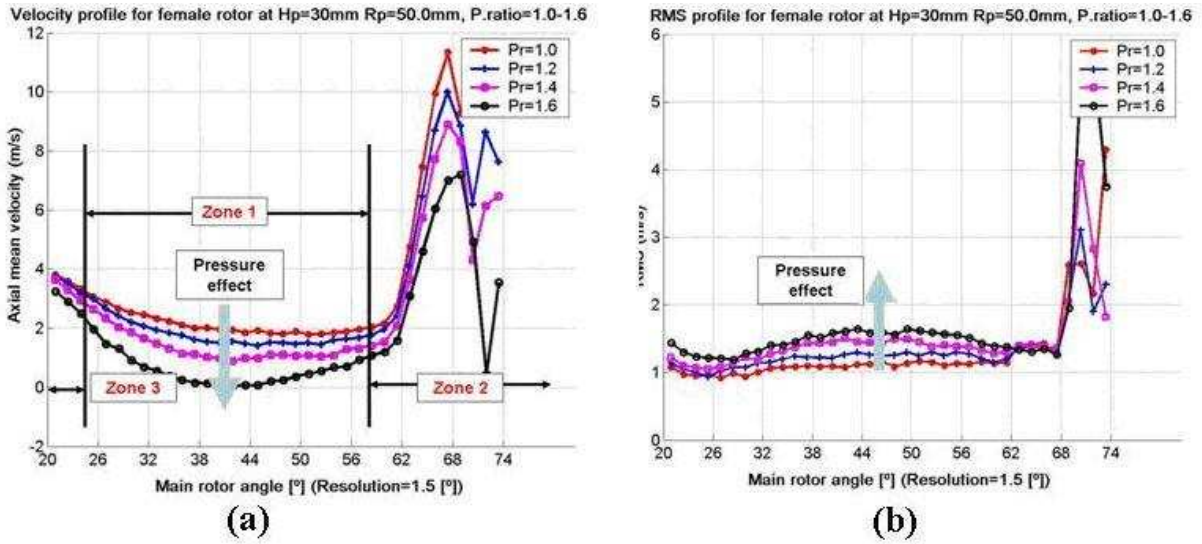


**Figure 11** Pressure influence in the female rotor: $R_p$=50.0mm and $H_p$=30mm: (a) axial mean velocity **(b)** axial RMS values.

Figure 11 shows the pressure influence for both velocity and turbulence curves on the female rotor. The control volume location is the same as in Figure 10. Four pressure ratios were taken, from 1.0 to 1.6, and the discharge temperature varies from 55ºC to 82ºC. Figure 11(a) shows strong influence of the pressure for zone 1 and 2 but only little changes on zone 3; in the latter zone the results confirm that flow motion is essentially driven by pressure difference between working chambers and temperature rather than other parameters. In additions, reduction in velocity on zone 2 is essentially due to smaller difference between exhaust pressure and internal compression. On Figure 11(b) RMS curves are presented and a higher pressure ratio leads to higher turbulence.

## CONCLUSIONS

Axial mean flow measurements and the corresponding turbulent fluctuations were characterised inside the rotor chamber at several cross sections of the screw compressor with high spatial and temporal resolution using laser Doppler velocimetry (LDV) at speed ranging from 800rpm to 1600 rpm and pressure ratio from 1 to 1.6. Here is a summary of the most important findings:

1 A temporal resolution of 0.1° of the rotor angle can be achieved, but the results of the axial mean and RMS velocities showed that the flow structure remained unchanged for an angular resolution of up to 1.5°. A high data rate pressure transducer was employed within the working chamber to provide an additional set of data to characterise not only the axial velocity field but also the instantaneous pressure.

2 The axial velocity distribution across the working chamber could be described by dividing the working chamber into three different zones: In zone 1, the bulk of the working chamber, the velocity is mainly influenced by the rotor motion; in zone 2, near the leading edge, the velocity is influenced mainly by the discharge process; in zone 3, near the trailing edge, it is influenced mainly by the leakages through the gaps between the rotors and the casing.

3 The temperature and compressor speed affect the losses in zone 3. In fact when the temperature rises, the thermal expansion of the rotor and the casing reduce the clearance leading to a decrease of the peak velocity close to the trailing edge.

4 The pressure measurements have confirmed that the air flow acceleration in zone 2 is strictly connected to the opening of the discharge port.

Overall, the obtained data will be used to establish a reliable CFD model of the flow and pressure distribution within twin screw machines, which, can then be used as a tool to further improve the design of screw compressors and expanders.

## ACKNOLEGEMENT

Financial support from EPSRC (Grant EP/C541456/1), Trane, Lotus and Gardner Denver is gratefully acknowledged. The authors would like to thank Tom Fleming, Michael Smith, Jim Ford and Grant Clow for their valuable technical support during the course of this work.

## REFERENCES

1. **Stosic N, 1998,** On gearing of helical screw compressor rotors, Proc IMechE, **212**(C), pp. 587-594.
2. **Nouri J.M., Guerrato D., Stosic N. and Kovacevic A., 2006,** Cycle-resolved velocity measurements within a screw compressor. 18th Int. Compressor Eng. Conf., 17-20 July 2006, Purdue.
3. **Nouri, J.M., Guerrato, D., Stosic N. and Arcoumanis C., 2007,** Axial Flow Characteristics within a Screw Compressor. Submitted to ASHRAE Research Journal.
4. **Kovacevic A., Stosic N. and Smith I.K., 2002**, CFD Analysis of Screw Compressor Performance. In: Advances of CFD in Fluid Machinery Design, edited by Elder R.L., A. Tourlidakis and M.K. Yates, Professional Engineering Publishing, London.
5. **Kampanis N., Arcoumanis C., Kato R., Kometani S., 2001,** Flow, combustion and emissions in a five-valve research gasoline engine. SAE Paper 2001-013556.
6. **Yan Y., Gashi S., Nouri J.M., Lockett R.D. and Arcoumanis C., 2005,** Investigation of spray characteristics in a spray guided DISI engine using PLIF and LDV, 2nd Int. Conference on Optical Diagnostics, ICOLD, London, September 2005.
7. **Liu C.H., Nouri J.M., Vafidis C. and Whitelaw J.H., 1990,** Experimental study of flow in a centrifugal pump, 5th International Symposium on Applications of Laser Techniques to Fluid Mechanics, Lisbon, July 1990.
8. **Arcoumanis C., Martinez-Botas R., Nouri J.M. and Su C.C., 1997,** Performance and exit flow characteristics of mixed flow turbines. International Journal of Rotating Machinery, **3**, No. 4, pp. 277-293.
9. **Arcoumanis C., Martinez-Botas R., Nouri J.M. and Su C.C., 1998,** Inlet and exit flow characteristics of mixed flow turbines. ASME, Int. gas Turbine and Aeroengine Congress and Exhibition, Paper 98-GT-495, Stockholm, June 1998.
10. **Zaidi S.H. and Elder, R.L., 1993,** Investigation of flow in a radial turbine using laser anemometry", ASME, Int. Gas Turbine and Aeroengine Congress and Exhibition, Cincinnati, paper 93-GT-55, Ohio, May 1993.
11. **Hockey R.M., Nouri J.M., 1996,** Turbulent flow in a baffled vessel strirred by a 60 pitched blade impeller. Chem. Eng. Science, **51**, pp. 4405-4421.